

Identifying topological excitonic insulators via bulk-edge correspondence

Hongwei Qu,¹ Zeying Zhang,² and Yuanchang Li^{1,*}

¹*Key Lab of advanced optoelectronic quantum architecture and measurement (MOE),
and Advanced Research Institute of Multidisciplinary Science,
Beijing Institute of Technology, Beijing 100081, China*

²*College of Mathematics and Physics,
Beijing University of Chemical Technology, Beijing 100029, China*

(Dated: December 20, 2024)

Abstract

Excitonic insulator remains elusive and there has been a lack of reliable identification methods. In this work, we demonstrate the promise of topological excitonic insulators for identification due to their unique bulk-edge correspondence, as illustrated by the LiFeX ($X = \text{S}, \text{Se}, \text{and Te}$) family. First-principles Bethe-Salpeter equation calculations reveal excitonic instabilities in these spin-orbit coupling quantum anomalous Hall insulators. Effective Hamiltonian analyses indicate that spontaneous exciton condensation does not disrupt the gapless edge state but reconstructs the bulk-gap to be almost independent of the spin-orbit coupling strength. This change in the bulk-edge correspondence can be experimentally inspected by angle-resolved photoelectron spectroscopy or electron compressibility measurements, providing observational evidence for the identification of topological excitonic insulators. Moreover, exciton condensation raises the critical temperature of the topological nontrivial phase above room temperature.

Excitonic insulator (EI) is a strongly correlated semiconductor that harbors spontaneously generated and condensed excitons (electron-hole pairs bound by Coulomb interactions)[1–5]. It is a macroscopic quantum system, akin to a superconductor, that essentially stems from many-body interactions among electrons. Instead of the excited states conventionally produced under energy injection, excitons now constitute the ground state of the system. This leads to a scarcity of suitable materials and difficulties in experimental identification[6–8]. Despite being pursued since its theoretical conception in the 1960s, there is currently no recognized EI. Thanks to recent advancements in computational science, a number of potential EIs have been predicted, and there is an urgent need to find reliable experimental methods for conclusive identification.

By definition, EIs are simply crystals where the exciton binding energy (E_b) exceeds the single-electron gap (E_g) at 0 K[4, 9]. Since E_b cannot be directly obtained experimentally, verifying EIs by their definition is not feasible. Contemporary verification of EIs utilizes phenomena derived from the phase transition induced by the spontaneous condensation of excitons. Typically, the excitonic transition leads to abrupt changes in crystal structure, frontier states, gap size, or optical properties that provide identifying signals[10–13]. However, none of these serve as a definitive “fingerprint”, and their presence only indicates the possibility of an EI. To achieve conclusive identification, all other competing mechanisms must be excluded, which is what makes EI identification so challenging. For example, $1T$ -TiSe₂ and Ta₂NiSe₅ are two highly interesting EI candidates. Since phase transitions are accompanied by structural distortions, there has been a debate on whether the driving force is the EI or the Jahn-Teller mechanism[6, 14, 15]. To circumvent this interference, researchers have turned to direct-gap semiconductors, and several EIs without structural distortions have been predicted[9]. However, in practice, it is still necessary to distinguish between single-electron and many-body gaps and exclude other possibilities such as Mott and disorder mechanisms[16, 17]. Although theoretical calculations can in principle help elucidate the gap nature, on the one hand, the EI theory involving quantum many-body problems is not well-established, and on the other hand, it is not realistic to rule out possible competing mechanisms one by one. Some researchers have attempted to probe EIs via superfluidity[18], yet such transport measurements are extremely difficult due to the charge-neutral nature of excitons. In fact, there is still controversy in the theoretical community about the existence of superfluidity in EIs[4, 14].

The interplay between strong electronic correlations and band topology opens up new research avenues and provides solutions to long-standing puzzles in condensed matter physics, such as the quantum anomalous Hall (QAH) effect[19]. Topological EI, which combines topological edge states and spontaneous exciton condensation of the bulk, has attracted intense attention from both the experimental and theoretical communities[13, 20–24]. Incorporating topology brings two additional advantages for identifying EI: i) The presence of nontrivial topology excludes some gap mechanisms and thus inherently circumvents their interference. ii) The unique bulk-edge correspondence of topological materials would provide useful insights into deciphering the gap nature.

In this work, we demonstrate how the bulk-edge correspondence enables us to distinguish between topological EIs and conventional spin-orbit coupling (SOC) topological insulators. We elaborate on this using the LiFeX ($X = \text{S, Se, and Te}$) family, which has been predicted to be SOC QAH insulators[25]. We perform first-principles calculations combined with the Bethe-Salpeter equation (BSE) to reveal excitonic instabilities in LiFeS and LiFeSe but not in LiFeTe. We then construct effective Hamiltonians to show that EI formation does not compromise gapless edge states. However, the bulk-gap reconfigured by exciton condensation becomes almost independent of the SOC strength, which is quite different from the linear growth upon SOC enhancement in SOC topological insulators. This difference in gap-SOC dependence can be evaluated experimentally by angle-resolved photoelectron spectroscopy or electron compressibility measurements[26], thus providing direct and unambiguous evidence for the identification of topological EIs. Finally, we assess the critical temperature of the EI phase to be over 400 K, which contributes to the operating temperature of the relevant QAH devices.

Density functional theory (DFT) calculations were performed within the Perdew-Burke-Ernzerhof (PBE) exchange-correlation functional[27] and the Heyd-Scuseria-Ernzerhof (HSE) hybrid functional[28] using the VASP code[29]. Electron-ion interaction was described by the projector augmented wave method[30, 31] with an energy cutoff of 350 eV. A vacuum layer of 20 Å was used to minimize spurious interactions between two neighboring images. A $15 \times 15 \times 1$ k -grid was used to find the geometric, electronic and magnetic ground state on the single-electron level. The excitonic properties were obtained by solving the BSE using the YAMBO code[32] with the single-electron band produced by the QUANTUM ESPRESSO package[33]. A fine $30 \times 30 \times 1$ k -grid, 300 bands and 10 Ry cutoff were

used to calculate the dielectric function matrix. Top four valence and bottom six conduction bands were included to build the BSE Hamiltonian. Given the computational cost, the BSE was solved on top of PBE band but with E_g corrected to the HSE value using a scissor operator for both the response function and diagonal part of the BSE kernel, which has been applied to study excitonic instabilities in low-dimensional materials[7–9, 17].

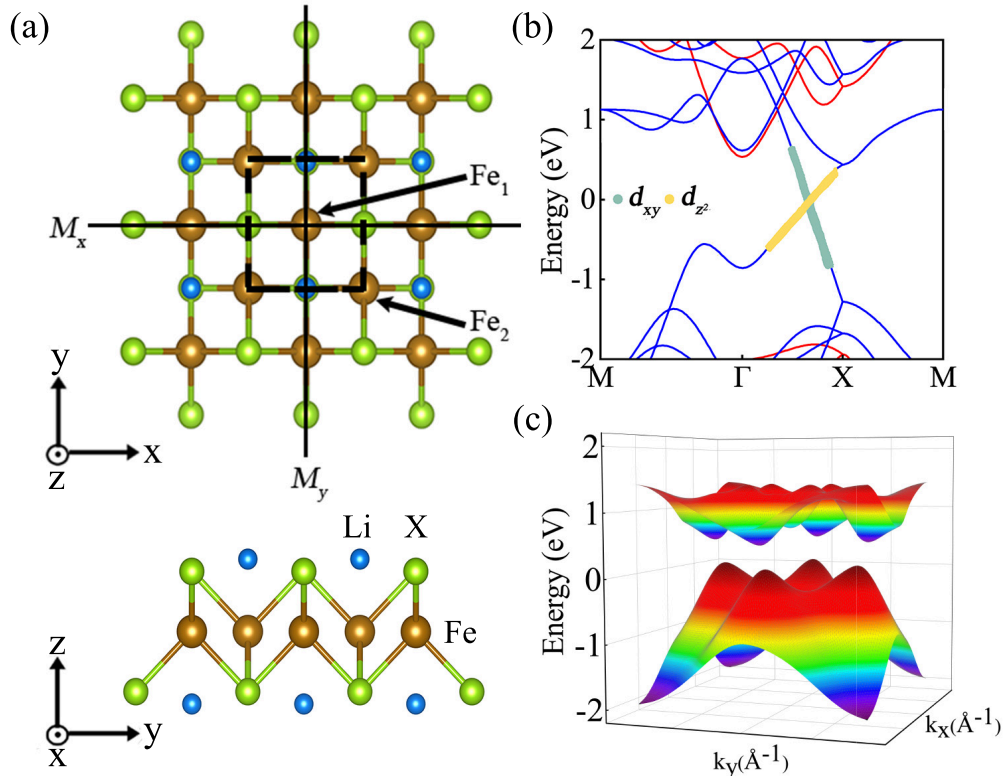


FIG. 1: (a) Top and side views of the monolayer LiFeX structure, which contains an out-of-plane Li-X-Fe-X-Li quintuple layer and an in-plane tetragonal lattice. The unit cell (black dashed rectangle) has two sets of Li, X and Fe atoms. The M_x and M_y lines represent the two mirror symmetries. (b) Spin-resolved band structure of LiFeSe without considering the SOC, as well as the orbital-projection of the linear Dirac-cone. Red and blue lines denote spin-majority and spin-minority, respectively. (c) Three-dimensional Dirac-cone band structure of LiFeSe in the entire Brillouin zone with the SOC included. In (b) and (c), the Fermi levels are set to zero.

The LiFeX exhibits a similar crystal structure, as depicted in Fig. 1(a). It is composed of a Li-X-Fe-X-Li quintuple layer with a tetragonal lattice in the $P4/nmm$ space group, forming a crystallographic monolayer containing two sets of Li, X, and Fe atoms. DFT and HSE calculations neglecting SOC both indicate that all three are 100% spin-polarized Dirac

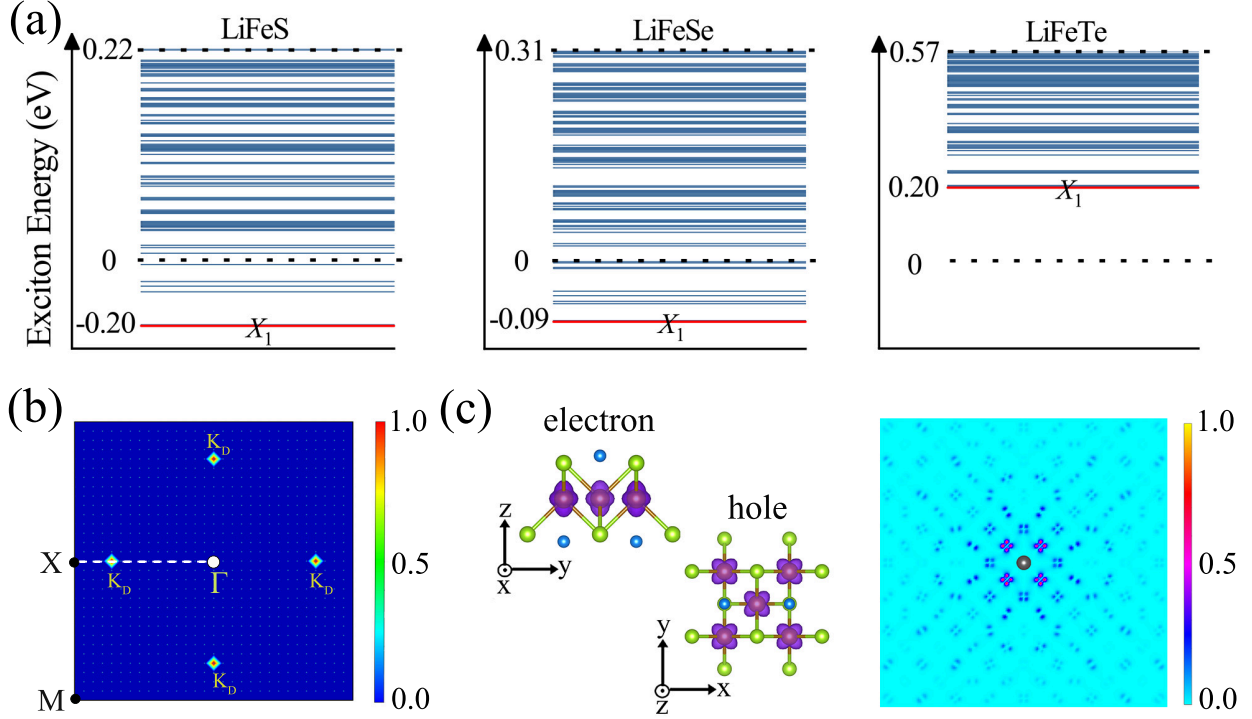


FIG. 2: (a) Exciton spectra of LiFeS, LiFeSe and LiFeTe obtained from solving the BSE. Each line denotes an exciton state and excitonic instability occurs if the lowest X_1 -exciton has a negative energy. (b) Wavefunction modulus of the X_1 -exciton in the reciprocal space for LiFeSe. (c) Plots of decomposed charge density for electrons and holes that make up the X_1 -excitons in LiFeSe with an isosurface of $0.1 \text{ e}/\text{\AA}^3$. (d) Wavefunction modulus of the X_1 -exciton in the real space for LiFeSe, with the hole fixed at the center (black dot). In (b) and (d), the maximum modulus has been renormalized to unity.

half-metals [see Fig. 1(b) and Fig. S1 of the Supplemental Material[34]] with an integer magnetic moment of $6 \mu_B$. There is a gap separated by Fe- d and X- s states for spin-majority while a linear Dirac-cone formed by Fe d_{xy} and d_{z^2} orbitals appears for spin-minority. A total of four Dirac-cones are found throughout the entire Brillouin zone and the degeneracy at the Dirac points originates from the mirror symmetry of M_x/M_y as shown in Fig. 1(a). When SOC is included, LiFeX displays a gap that depends on the easy magnetization axis. An out-of-plane easy axis breaks the M_x/M_y symmetry, enabling d_{xy} and d_{z^2} hybridization to generate a gap. In contrast, an in-plane easy axis does not gap the Dirac-cone. Our HSE calculations reveal that LiFeS, LiFeSe, and LiFeTe all have out-of-plane easy axes that

open gaps of 0.22, 0.31, and 0.57 eV, as shown in Fig. 1(c) and Fig. S1[34]. Given that Dirac half-metal is a natural avenue toward the QAH effect[35], we conduct Berry curvature calculations and find that each gapped Dirac-cone contributes a quantized Berry phase of π . Consequently, we obtain a Chern number of $C = 2$, indicating that all three LiFeX are SOC QAH insulators, consistent with previous study[25].

The Dirac-cone band, monolayer structure, and the predominance of d contributions near the Fermi energy all suggest a weak electron-hole screening interaction in LiFeX. This naturally gives rise to significant excitonic effects. We have thus solved the BSE for the low-energy excitation spectrum as shown in Fig. 2(a). It can be seen that the lowest X_1 -excitons have energies (E_t) of -0.20 and -0.09 eV in LiFeS and LiFeSe, respectively, and 0.20 eV in LiFeTe. A negative E_t indicates excitonic instability, meaning that the X_1 -excitons form spontaneously without the need of energy input. These excitons will condense and reconstruct a many-body gap below the critical temperature. Hence, LiFeS and LiFeSe possess fundamentally different bulk insulating gaps compared to LiFeTe.

Taking LiFeSe as an example, Fig. 2(b) plots the wavefunction of the X_1 -exciton in reciprocal space. It is almost completely distributed around the four gapped Dirac points, which is characteristic of the Wannier-Mott exciton. Thus, the X_1 -exciton has a well-defined E_b equal to the difference between the corresponding E_g and E_t . For LiFeS, LiFeSe, and LiFeTe, the resulting values are 0.42, 0.40, and 0.37 eV, respectively. All E_b are around 0.4 eV, partly because the difference in E_g is not significant, and more likely because the unique nonlocal screening in the monolayer is less sensitive to the constituent elements[9, 36]. Figure 2(c) shows the charge densities of the electron and hole that make up the X_1 -exciton. The electron displays a d_{z^2} feature while the hole displays a d_{xy} feature. Despite being highly localized in the reciprocal space, the X_1 -exciton extends over a large distance in real space as shown in Fig. 2(d). At the same time, however, the modulus of the electron wavefunction decays rapidly away from the hole, with the intensity mainly concentrated on the neighbouring Fe. In the single-electron picture, two neighbouring Fe atoms are identical. In the excitonic phase, one assumes a hole while the other assumes an electron due to the spontaneous formation of X_1 -excitons. As a result, the spatial inversion symmetry is spontaneously broken[8, 17, 23].

Next, we explore the properties of EI ground states. We start with the impact of excitonic phase transitions on topological edge states. Based on the aforementioned first-principles

BSE results, we construct an effective Hamiltonian in the basis $\{|Fe_1, d_{xy}\rangle, |Fe_1, d_{z^2}\rangle, |Fe_2, d_{xy}\rangle, |Fe_2, d_{z^2}\rangle\}$

$$H(\vec{k}) = H_0 + H_{\text{soc}} + H_{\text{eh}} = \begin{pmatrix} \epsilon_1 & 0 & \vec{t}_1 & \vec{t}_2 \\ 0 & \epsilon_2 & \vec{t}_2 & \vec{t}_3 \\ \vec{t}_1 & \vec{t}_2 & \epsilon_1 & 0 \\ \vec{t}_2 & \vec{t}_3 & 0 & \epsilon_2 \end{pmatrix} + \begin{pmatrix} 0 & -\vec{r} & 0 & 0 \\ \vec{r} & 0 & 0 & 0 \\ 0 & 0 & 0 & -\vec{r} \\ 0 & 0 & \vec{r} & 0 \end{pmatrix} + \begin{pmatrix} 0 & 0 & 0 & \vec{\Lambda}_1 \\ 0 & 0 & \vec{\Lambda}_2 & 0 \\ 0 & \vec{\Lambda}_2 & 0 & 0 \\ \vec{\Lambda}_1 & 0 & 0 & 0 \end{pmatrix}. \quad (1)$$

Here, H_0 and H_{soc} are formulated in the tight-binding approximation using the MagneticTB package[37] developed by one of the authors. The parameters $\epsilon_{1(2)}$, $\vec{t}_{1(2,3)}$ and \vec{r} represent the orbital energy, hopping and SOC parameters, respectively. For more details, see the Supplemental Material[34]. H_{eh} describes the effect of X_1 -excitons, which stems from two facts of the first-principles result: (i) It involves the pairing between d_{xy} and d_{z^2} of Fe_1 and Fe_2 . (ii) The equivalence of Fe_1 and Fe_2 is broken, so $\vec{\Lambda}_1$ and $\vec{\Lambda}_2$ must be different. For simplicity, let $\vec{\Lambda}_1 = 0$.

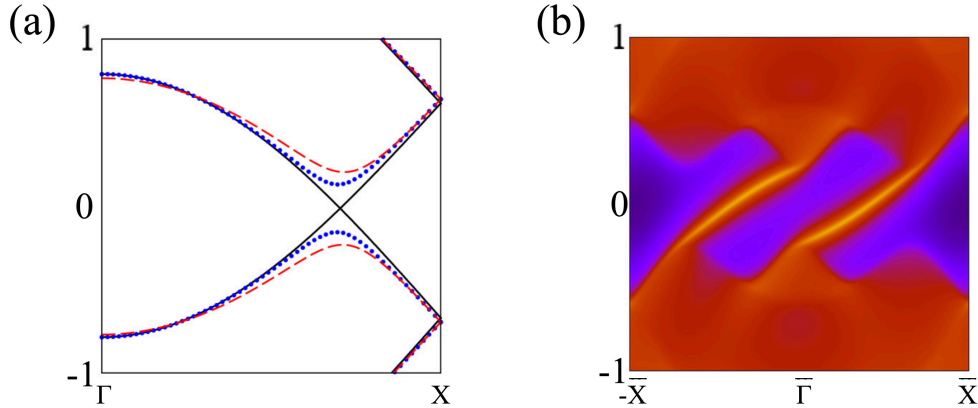


FIG. 3: (a) Band structures derived from $H(\vec{k})$ under different scenarios, namely, H_0 (black lines), H_0+H_{soc} (blue dots), and $H_0+H_{\text{soc}}+H_{\text{eh}}$ (red dashes). See the Supplementary Material[34] for more details. (b) Edge modes obtained from $H_0+H_{\text{soc}}+H_{\text{eh}}$, where there are two gapless edge states (bright yellow lines) connecting the conduction and valence bands. The Fermi levels are set to zero.

Figure 3(a) depicts the bands derived from $H(\vec{k})$ under different scenarios. When only H_0 is considered, a Dirac-cone appears (black lines). Adding H_{soc} lifts the degeneracy of the Dirac point and creates a gap (blue dots), which is further enlarged by H_{eh} (red dashes). These findings are in good agreement with the first-principles results. Subsequently, we

compute the edge states using the Hamiltonian (1) with and without H_{eh} , respectively, and the results are shown in Fig. 3(b) and Fig. S2 of the Supplementary Material[34]. It is evident that the inclusion of H_{eh} gives two edge states connecting the conduction and valence bands, corresponding to a Chern number of $C = 2$. This feature is the same as that without H_{eh} (see Fig. S2), which characterizes the SOC QAH phase. Thus, the excitonic phase transition does not compromise the gapless edge states of the SOC QAH phase. In other words, the EI phase remains topologically nontrivial. This finding is of great scientific significance. It demonstrates that excitonic instability in SOC topological insulators leads to topological EIs without causing a topological phase transition, validating previous speculations[23, 38].

We proceed to study the bulk-gap of the EI phase using a simple two-band effective Hamiltonian

$$\hat{H} = \sum_{\vec{k}} [\varepsilon_a(\vec{k}) - \mu] a_{\vec{k}}^+ a_{\vec{k}} + \sum_{\vec{k}} [\varepsilon_b(\vec{k}) - \mu] b_{\vec{k}}^+ b_{\vec{k}} + \frac{1}{2S} \sum_{\vec{k}', \vec{k}, \vec{q}} [V_{aa}(\vec{q}) a_{\vec{k}+\vec{q}}^+ a_{\vec{k}'-\vec{q}}^+ a_{\vec{k}} a_{\vec{k}} + V_{bb}(\vec{q}) b_{\vec{k}+\vec{q}}^+ b_{\vec{k}'-\vec{q}}^+ b_{\vec{k}} b_{\vec{k}} - 2V_{ab}(\vec{q}) a_{\vec{k}+\vec{q}}^+ b_{\vec{k}'-\vec{q}}^+ b_{\vec{k}} a_{\vec{k}}], \quad (2)$$

where μ and S are the chemical potential and the in-plane area. $a_{\vec{k}}$ ($a_{\vec{k}}^\dagger$) and $b_{\vec{k}}$ ($b_{\vec{k}}^\dagger$) are the destruction (creation) operators of electron and hole. $\varepsilon_a(\vec{k}) = \frac{\hbar^2 \vec{k}^2}{2m_e} + \frac{E_g}{2}$ and $\varepsilon_b(\vec{k}) = -\frac{\hbar^2 \vec{k}^2}{2m_h} - \frac{E_g}{2}$ denote the conduction and valence band[7, 36], with electron (hole) effective mass m_e (m_h) and E_g fitted from our first-principles calculations. $V(\vec{q})$ denotes the many-body interactions, i.e., $V(\vec{q}) = V_{aa}(\vec{q}) = V_{bb}(\vec{q}) = V_{ab}(\vec{q}) = \frac{2\pi}{(1+2\pi\alpha_{2D}|q|)|q|}$, with two-dimensional polarizability α_{2D} obtained from first-principles calculations. Using the Hartree-Fock approximation and $\frac{\varepsilon_a(\vec{k}) + \varepsilon_b(\vec{k})}{2} = 0$ [39], we derive the coupled equations

$$\begin{aligned} \Delta_{cv}(\vec{k}) &= \frac{1}{2S} \sum_{\vec{k}'} V(\vec{k} - \vec{k}') \frac{\Delta_{cv}(\vec{k}')}{E(\vec{k}')}, \\ \xi(\vec{k}) &= \frac{\varepsilon_a(\vec{k}) - \varepsilon_b(\vec{k})}{2} - \frac{1}{2S} \sum_{\vec{k}'} V(\vec{k} - \vec{k}') (1 - \frac{\xi(\vec{k}')}{E(\vec{k}')}), \\ E_c(\vec{k}) &= -E_v(\vec{k}) = \sqrt{\xi^2(\vec{k}) + \Delta_{cv}^2(\vec{k})}. \end{aligned} \quad (3)$$

We then solve Eqs. (3) self-consistently to obtain the minimum values of $\min[\Delta_{cv}(\vec{k})]$ and $\min[\xi(\vec{k})]$, which are the many-body gap and bulk-gap of the EI phase.

Figure 4(a) summarizes the bulk-gap of LiFeX opened by SOC and excitons, respectively. Note that LiFeTe does not have excitonic instability. Here, we have further established a gap-SOC curve by linearly interpolating the first-principles results of LiFeS, LiFeSe, and LiFeTe

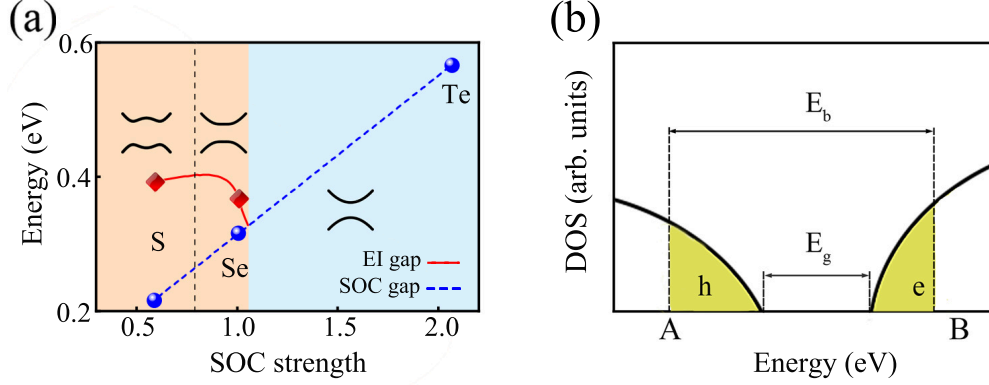


FIG. 4: (a) Bulk-gaps of the LiFeX family as a function of SOC strength. The SOC bulk-gaps are obtained by first-principles (Blue balls), while the EI ones (Red diamonds) of LiFeS and LiFeSe are obtained by self-consistently solving Eqs. (3). The orange and blue regions indicate that the ground state of the system is a topological EI and SOC topological insulator, respectively. Insets show the characteristic band structure in the ground state. Note that a change in the characteristic band structure occurs at the location of the black vertical dashed line in the topological EI phase. Dependence curves are established by linearly interpolating the first-principles results of LiFeS, LiFeSe, and LiFeTe in order to simulate the effect of possible S -group atom alloying. See the Supplementary Material[34] for more details. (b) A schematic for estimating the exciton density n using the rigid-band approximation based on the first-principles density of states (DOS). It is assumed that spontaneous condensation of excitons only affects states in the E_b range. Furthermore, to ensure that the exciton is charge neutral, the number of electrons (e) and holes (h) must be equal, i.e., the area of the yellow shaded regions in the valence and conduction bands are equal. With these two points, the locations of points A and B can be uniquely determined to obtain n .

in order to simulate the effect of possible fine-tuning the SOC strength through S -group atom alloying in the experiment[40]. See the Supplementary Material[34] for details. It can be seen that the bulk-gaps of the EI and SOC phases exhibit quite different dependence behaviours. When LiFeX is in the SOC QAH phase, the bulk-gap increases linearly as the SOC increases from S to Se to Te. In contrast, when LiFeX is in the topological EI phase, the bulk-gap varies much less with SOC. When LiFeX are all in their own ground states, their bulk-gaps have a LiFeTe $>$ LiFeS $>$ LiFeSe relationship, which is distinctly different from that in the SOC topological phase, where LiFeTe $>$ LiFeSe $>$ LiFeS. The difference

is also reflected in the variation trend. While replacing Se with Te in LiFeSe increases the SOC, the EI bulk-gap decreases until the excitonic instability disappears. This qualitative difference thus allows a clear experimental determination of whether LiFeX is in the EI state.

Exciton condensation to reconfigure the bulk-gap inevitably produces a very different bulk-edge correspondence from that of the SOC topological insulator. Therefore, identifying topological EIs via such a change is generally valid and not limited to the LiFeX family. In particular, first-principles calculations, which enjoy great success in predicting and confirming topological materials, can contribute to topological EIs as well. When the emergence of gapless edge states locks the system in a topological phase, the bulk-gap may come from either the SOC or the exciton. In the former case, the bulk-gap necessarily increases with increasing SOC strength, so that the heavier the constituent element, the larger the bulk-gap[40]. In the latter case, the bulk-gap is approximated by E_b , which depends on the overall screening effect of the system. For low-dimensional materials, it is not sensitive to the constituent elements[16, 23, 41]. Therefore, topological EIs can be unambiguously identified by modulating the system SOC strength through substituting elements of the same group and then monitoring the gap-SOC dependence. Bulk-gaps that vary significantly and monotonically with SOC are SOC topological insulators, whereas those that do not vary much and have no significant dependence are topological EIs.

Within the excitonic QAH (topological EI) phase, the gapless edge states are protected by the many-body gap rather than the transport gap (bulk-gap)[42]. At this point, the critical temperature T_c is determined when $\min[\Delta_{cv}(\vec{k})] = 0$. Multiplying Eqs. (3) by the temperature factor $(\frac{1}{e^{\frac{E_v}{k_B T}} - 1} - \frac{1}{e^{\frac{E_c}{k_B T}} - 1})$ [7], we can estimate the T_c of LiFeS and LiFeSe as 1050 and 400 K, respectively. Hence, QAH devices based on LiFeS and LiFeSe are expected to operate at temperatures above room temperature. More interestingly, the formation of EI leads to a much higher operating temperature for LiFeS than for LiFeSe, which is an opposite trend to that of SOC topological insulators. This not only provides evidence for the EI identification, but also indicates that lighter elements are more favourable for topological EIs, which greatly complements the selection range of SOC topological materials.

Above estimation treats the spontaneously formed excitons as a weakly interacting boson

gas. If treated as an ideal boson gas, the T_c can be calculated using the statistical formula[43]

$$n = \frac{mk_B T_c}{2\pi\hbar^2} \sum_{j=1}^{\infty} \frac{(e^{-|E_t|/k_B T_c})^j}{j}, \quad (4)$$

where m and n are exciton mass and density, respectively. The former is obtained by fitting first-principles results, while the latter is estimated in two ways. One uses Eqs. (3), i.e., $n^{\text{mod}} = \sum_{\vec{k}} \frac{|\Delta_{cv}(\vec{k})|^2}{S}$ [20, 39, 44]. It leads to $n^{\text{mod}} = 1.3 \times 10^{12}$ and $9.7 \times 10^{10} \text{ cm}^{-2}$ for LiFeS and LiFeSe, respectively, which corresponds to $T_c^{\text{mod}} = 1126$ and 334 K. Compared to the results for the interacting boson gas described above, the inter-exciton interactions lead to a 76 K decrease in T_c for LiFeS and a 66 K increase in T_c for LiFeSe.

The other uses a rigid band approximation as depicted in Fig. 4(b). It consists of two points: (i) Assuming that the exciton reconstruction involves only the E_b energy range and nowhere else. (ii) Charge neutrality of the exciton requires an equal number of electrons and holes, i.e., an equal area of the electron and hole regions. Together, these two conditions determine the A and B points in Fig. 4(b), giving $n^{\text{rig}} = 3.5 \times 10^{12}$ and $1.3 \times 10^{12} \text{ cm}^{-2}$ for LiFeS and LiFeSe, respectively. They yield $T_c^{\text{rig}} = 1585$ and 734 K.

Comparing n^{rig} and T_c^{rig} with the preceding results, it can be seen that the effect of band relaxation is much larger than that of inter-exciton interactions. Band relaxation leads to an order-of-magnitude decrease in n for LiFeSe, reducing T_c by more than 50%. For LiFeS, this effect is relatively small, with n and T_c being reduced by $\sim 60\%$ and $\sim 30\%$, respectively. Generally speaking, band relaxation depends on $|E_t|$. The larger $|E_t|$ is, the larger the contribution away from the band edges [Boundaries between the yellow and white regions in Fig. 4(b)] is, and the smaller the relaxation effect is. Since $|E_t|$ for LiFeS is more than twice as large as that for LiFeSe, the relaxation effect is weaker for the former.

In summary, our first-principles BSE calculations reveal excitonic instabilities in the SOC QAH insulators LiFeS and LiFeSe. Subsequent effective Hamiltonian studies show that the gapless edge state remains intact in the presence of spontaneous exciton condensation. However, the bulk-gap reformulation leads to a different bulk-edge correspondence, which can be experimentally inspected by measuring the gap-SOC dependence. Although the findings are drawn from the LiFeX family, the underlying principle is broadly applicable to the identification of topological EIs. Our work not only makes progress toward solving a long-standing challenge of unambiguously identifying EIs, but also offers new perspectives on enhancing the operational temperature of QAH devices.

Y.L. thanks Z. Liu and X. M. Zhang for a useful discussion. This work was supported by the Ministry of Science and Technology of China (Grant Nos. 2023YFA1406400 and 2020YFA0308800), the National Natural Science Foundation of China (Grant No. 12074034), and the Fundamental Research Funds for the Central Universities (No. ZY2418).

* Electronic address: yuancli@bit.edu.cn

- [1] Mott, N, The Transition to the Metallic State. *Philosophical Magazine*, **6**, 287 (1961) .
- [2] R. S. Knox, in *Solid State Physics*, edited by F. Seitz and D. Turnbull (Academic Press, New York, 1963), Suppl. 5, p. 100.
- [3] D. Jérôme, T. M. Rice, and W. Kohn, Excitonic Insulator, *Phys. Rev.* **158**, 462 (1967).
- [4] B. I. Halperin and T. M. Rice, Possible anomalies at a semimetal-semiconductor transition, *Rev. Mod. Phys.* **40**, 755 (1968).
- [5] R. R. Guseinov and L. V. Keldysh, Nature of the Phase Transition under the Conditions of an “Excitonic” Instability in the Electronic Spectrum of a Crystal, *Sov. Phys. JETP* **36**, 1193 (1973).
- [6] A. Kogar, S. Vig, M. S. Rak, A. A. Husain, F. Flicker, Y. I. Joe, L. Venema, G. J. MacDougall, T. C. Chiang, E. Fradkin, J. van Wezel, and P. Abbamonte, Signatures of exciton condensation in a transition metal dichalcogenide, *Science* **358**, 1314 (2017).
- [7] Z. Y. Jiang, W. K. Lou, Y. Liu, Y. C. Li, H. F. Song, K. Chang, W. H. Duan, and S. B. Zhang, Spin-triplet excitonic insulator: The case of semihydrogenated graphene, *Phys. Rev. Lett.* **124**, 166401 (2020).
- [8] Z. Y. Jiang, Y. C. Li, W. H. Duan, and S. B. Zhang, Half-excitonic insulator: A single-spin Bose-Einstein condensate, *Phys. Rev. Lett.* **122**, 236402 (2019).
- [9] Z. Y. Jiang, Y. C. Li, S. B. Zhang, and W. H. Duan, Realizing an intrinsic excitonic insulator by decoupling exciton binding energy from the minimum band gap, *Phys. Rev. B* **98**, 081408(R) (2018).
- [10] B. Bucher, P. Steiner, and P. Wachter, Excitonic insulator phase in $\text{TmSe}_{0.45}\text{Te}_{0.55}$, *Phys. Rev. Lett.* **67**, 2717 (1991).
- [11] H. Cercellier, C. Monney, F. Clerc, C. Battaglia, L. Despont, M. G. Garnier, H. Beck, P. Aebi, L. Patthey, H. Berger, and L. Forró, Evidence for an Excitonic Insulator Phase in $1T\text{-TiSe}_2$,

- Phys. Rev. Lett. **99**, 146403 (2007).
- [12] Y. Wakisaka, T. Sudayama, K. Takubo, T. Mizokawa, M. Arita, H. Namatame, M. Taniguchi, N. Katayama, M. Nohara, and H. Takagi, Excitonic Insulator State in Ta_2NiSe_5 Probed by Photoemission Spectroscopy, Phys. Rev. Lett. **103**, 026402 (2009).
- [13] L. Du, X. Li, W. Lou, G. Sullivan, K. Chang, J. Kono, and R. R. Du, Evidence for a topological excitonic insulator in InAs/GaSb bilayers. Nat. Commun. **8**, 1971 (2017).
- [14] G. Mazza, M. Rösner, L. Windgätter, S. Latini, H. Hübener, A. J. Millis, A. Rubio, and A. Georges, Nature of Symmetry Breaking at the Excitonic Insulator Transition: Ta_2NiSe_5 , Phys. Rev. Lett. **124**, 197601 (2020).
- [15] M. M. Guo and Y. C. Li, Electronic and optical properties of a Ta_2NiSe_5 monolayer: A first-principles study, Appl. Phys. Lett. **125**, 253105 (2024).
- [16] J. Liu, G.-B. Liu, and Y. C. Li, Electric-field-driven excitonic instability in an organometallic manganese-cyclopentadienyl wire, Phys. Rev. B **104**, 085150 (2021).
- [17] Varsano, S. Sorella, D. Sangalli, M. Barborini, S. Corni, E. Molinari, and M. Rontani, Carbon nanotubes as excitonic insulators, Nat. Commun. **8**, 1461 (2017)
- [18] X. M. Liu, J. I. A. Li, K. Watanabe, T. Taniguchi, J. Hone, B. I. Halperin, P. Kim, and C. R. Dean, Crossover between strongly coupled and weakly coupled exciton superfluids, Science **375**, 205 (2022).
- [19] C.-Z. Chang, C.-X. Liu, and A. H. MacDonald, Colloquium: Quantum anomalous Hall effect, Rev. Mod. Phys. **95**, 011002 (2023).
- [20] D. Varsano, M. Palummo, E. Molinari, and M. Rontani, A monolayer transition-metal dichalcogenide as a topological excitonic insulator, Nat. Nanotechnol. **15**, 367 (2020).
- [21] Y. Jia, P. Wang, C. Chiu, Z. Song, G. Yu, B. Jäck, S. Lei, S. Klemenz, F. A. Cevallos, M. Onyszczak, N. Fishchenko, X. Liu, G. Farahi, F. Xie, Y. Xu, K. Watanabe, T. Taniguchi, B. A. Bernevig, R. J. Cava, L. M. Schoop, A. Yazdani, and S. Wu, Evidence for a monolayer excitonic insulator, Nat. Phys. **18**, 87 (2022).
- [22] B. Sun, W. Zhao, T. Palomaki, Z. Fei, E. Runburg, P. Malinowski, X. Huang, J. Cenker, Y. T. Cui, J. H. Chu, X. Xu, S. S. Ataei, D. Varsano, M. Palummo, E. Molinari, M. Rontani, and D. H. Cobden, Evidence for equilibrium exciton condensation in monolayer WTe_2 , Nat. Phys. **18**, 94 (2022).
- [23] S. Dong and Y. C. Li, Robust high-temperature topological excitonic insulator of transition-

- metal carbides (MXenes), Phys. Rev. B **107**, 235147 (2023).
- [24] H. Yang, J. Zeng, Y. Shao, Y. Xu, X. Dai, and X. Z. Li, Spin-triplet topological excitonic insulators in two-dimensional materials, Phys. Rev. B **109**, 075167 (2024).
- [25] Yang Li, Jiaheng Li, Yang Li, Meng Ye, Fawei Zheng, Zetao Zhang, Jingheng Fu, Wenhui Duan, and Yong Xu, High-temperature quantum anomalous Hall insulators in lithium-decorated iron-based superconductor materials, Phys. Rev. Lett. **125**, 086401 (2020).
- [26] A. F. Young, J. D. Sanchez-Yamagishi, B. Hunt, S. H. Choi, K. Watanabe, T. Taniguchi, R. C. Ashoori, and P. Jarillo-Herrero, Tunable symmetry breaking and helical edge transport in a graphene quantum spin Hall state, Nature **505**, 528 (2014).
- [27] J. P. Perdew, K. Burke, and M. Ernzerhof, Generalized Gradient Approximation Made Simple, Phys. Rev. Lett. **77**, 3865 (1996).
- [28] J. Heyd, G. E. Scuseria, and M. Ernzerhof, Hybrid functionals based on a screened Coulomb potential, J. Chem. Phys. **118**, 8207 (2003); **124**, 219906(E) (2006).
- [29] G. Kresse and J. Furthmüller, Efficient iterative schemes for *abinitio* total-energy calculations using a plane-wave basis set, Phys. Rev. B **54**, 11169 (1996).
- [30] P.E. Blöchl, Projector augmented-wave method, Phys. Rev. B **50**, 17953 (1994).
- [31] G. Kresse and D. Joubert, From ultrasoft pseudopotentials to the projector augmented-wave method, Phys. Rev. B **59**, 1758 (1999).
- [32] D. Sangalli, A. Ferretti, H. Miranda, C. Attaccalite, I. Marri, E. Cannuccia, P. Melo, M. Marsili, F. Paleari, A. Marrazzo et al., Many-body perturbation theory calculations using the yambo code, J. Phys.: Condens. Matter **31**, 325902 (2019).
- [33] P. Giannozzi, S. Baroni, N. Bonini, M. Calandra, R. Car, C. Cavazzoni, D. Ceresoli, G. L. Chiarotti, M. Cococcioni, I. Dabo, A. D. Corso, S. de Gironcoli, S. Fabris, G. Fratesi, R. Gebauer, U. Gerstmann, C. Gougoussis, A. Kokalj, M. Lazzeri, L. Martin-Samos et al., QUANTUM ESPRESSO: A modular and open-source software project for quantum simulations of materials, J. Phys.: Condens. Matter **21**, 395502 (2009).
- [34] See the Supplemental Material for HSE band structures of LiFeX, details of the effective Hamiltonian calculations, and the establishment of gap-SOC curve.
- [35] Y. C. Li, D. West, H. Q. Huang, J. Li, S. B. Zhang, and W. H. Duan, Theory of the Dirac half metal and quantum anomalous Hall effect in Mn-intercalated epitaxial graphene, Phys. Rev. B **92**, 201403(R) (2015).

- [36] Z. Y. Jiang, Z. R. Liu, Y. C. Li, and W. H. Duan, Scaling Universality between Band Gap and Exciton Binding Energy of Two-Dimensional Semiconductors, *Phys. Rev. Lett.* **118**, 266401 (2017).
- [37] Z. Y. Zhang, Z.-M. Yu, G.-B. Liu, and Y. G. Yao, MagneticTB: A package for tight-binding model of magnetic and non-magnetic materials. *Comput. Phys. Commun.* **270**, 108153 (2022).
- [38] F.-C. Wu, F. Xue, and A. H. MacDonald, Theory of two-dimensional spatially indirect equilibrium exciton condensates, *Phys. Rev. B* **92**, 165121 (2015).
- [39] F. Xue and A. H. MacDonald, Time-Reversal Symmetry-Breaking Nematic Insulators near Quantum Spin Hall Phase Transitions, *Phys. Rev. Lett.* **120**, 186802 (2018).
- [40] Su-Yang Xu, Y. Xia, L. A. Wray, S. Jia, F. Meier, J. H. Dil, J. Osterwalder, B. Slomski, A. Bansil, H. Lin, R. J. Cava, M. Z. Hasan, Topological Phase Transition and Texture Inversion in a Tunable Topological Insulator, *Science* **232**, 560 (2011).
- [41] S. Dong and Y. C. Li, Transition from band insulator to excitonic insulator via alloying Se into monolayer TiS_3 : A computational study, *Phys. Rev. B* **102**, 155119 (2020)
- [42] P. Z. Mai, J. C. Zhao, T. A. Maier, B. Bradlyn, and Philip W. Phillips, Topological phase transition without single particle gap closing in strongly correlated systems, *Phys. Rev. B* **110**, 075105 (2024).
- [43] J. Liu, H. Qu, and Y. C. Li, One-Dimensional Magnetic Excitonic Insulators, *New J. Phys.* **26**, 103034 (2024).
- [44] S. S. Ataei, D. Varsano, E. Molinari, and M. Rontani, Evidence of ideal excitonic insulator in bulk MoS_2 under pressure, *Proc. Natl. Acad. Sci. USA* **118**, e2010110118 (2021).